applied sciences

MDPI

Article

Facile Fabrication of Superhydrophobic and Superoleophilic Polyurethane Foil with Micropillar and Microporous Structures for Efficient Oil/Water Separation

Weibin Wu [1,2,*], Mingjin Xu [3], Qinqin Wang [1,2], Xue Yang [1,2] and Changgeng Shuai [1,2]

[1] Institute of Noise & Vibration, Naval University of Engineering, Wuhan 430033, China; yang2014xue@163.com (X.Y.); chgshuai@163.com (C.S.)
[2] National Key Laboratory on Ship Vibration & Noise, Wuhan 430033, China
[3] College of Naval Architecture and Ocean Engineering, Naval University of Engineering, Wuhan 430033, China; xumingjinnudt@163.com
* Correspondence: wuweibin0910@163.com

Abstract: Oil spill cleanup in water remains a critical challenge due to the harmful secondary pollution from conventional methods such as burning or chemical degradation. Herein, we present a facile method to fabricate a superhydrophobic and superoleophilic polyurethane (PU) foil for efficient and environmentally friendly oil/water separation. More specifically, micropillar arrays were embedded onto the foil surface through a nanoimprinting process. Microporous structures were generated at the foil cross-section by a supercritical carbon dioxide (CO_2) saturation method. The dimensions of pillar and pore structures were optimized with the aim of boosting selective wetting (i.e., water repellency and oil attraction) properties. As a result, the developed PU foil shows an oil absorption efficiency nearly 4 times higher than a pristine reference. Moreover, the structured PU foil stably retains the absorbed oil for over a week, demonstrating an absorption capacity of nearly 400%, which is also much superior than the unstructured sample. Our concept of combining both topographical micropillars and cross-sectional micropores onto PU foil provides a novel approach for achieving efficient and environmental friendly oil/water separation.

Keywords: superhydrophobicity; oil/water separation; micropillar; microporous; foil

Citation: Wu, W.; Xu, M.; Wang, Q.; Yang, X.; Shuai, C. Facile Fabrication of Superhydrophobic and Superoleophilic Polyurethane Foil with Micropillar and Microporous Structures for Efficient Oil/Water Separation. *Appl. Sci.* **2024**, *14*, 3935. https://doi.org/10.3390/app14093935

Academic Editors: Ana Martins Amaro and Mohamed Khayet

Received: 14 March 2024
Revised: 1 May 2024
Accepted: 3 May 2024
Published: 5 May 2024

1. Introduction

Accidental oil spillage has become a serious public problem as it has a severe negatively impact on aquatic safety and human health [1,2]. Conventional techniques for oil spill cleanup mainly include in situ burning, chemical degradation [3,4] and membrane filtration [5,6]. However, burning or degradation usually causes potentially harmful residues, whereas the filtration method requires the collection of oil/water mixtures into the filtration setup by extra facilities such as pumps and containers. These methods are usually inconvenient for engineering applications. Thus, it is of great significance to develop a facile and sustainable approach for oil/water separation to tackle the oil pollution challenge.

Cleaning oil by absorption [7,8] is a promising method without secondary pollution or the need for extra facilities, which is favorable for practical applications. The used sorbents are generally required to repel water but absorb oil (i.e., superhydrophobic/superoleophilic) [9] to accomplish efficient oil/water separation. Besides this, they should also possess characteristics of high absorption capacity and upscalable fabrication [10]. Researchers first investigated such materials from nature due to their potential benefits of low cost and large amount. Oil-absorbing materials including straw soot [11], carbon oxide [12], fly ash [13], and zeolites [14] have been reported. Nonetheless, shortcomings of low absorption capability and environmental incompatibility of these materials impede their upscaled industrial use [13]. Currently, superhydrophobic or superoleophilic

sorbents are commonly artificially synthesized by modifying the chemical composition of materials with low surface energy or constructing a rough topography. According to the type of substrate, they are classified into fiber materials [15], aerogel materials [16], resin materials [17], etc. In most cases, these technical materials are fabricated as polymeric sponges [18–20], specially coated metal meshes [21–23], or metal-coated fabrics [5] by various chemical methods. The chemical substances used in their production [18] and disposal [21], however, might also cause toxic pollution. Alternatively, topographical structures, due to their easy fabrication and being environmental benign, producing no chemical residues, have gained more and more attention for oil/water separation applications.

The most well-known example of a topographically structured oil/water separator from nature is the water-repellent leaves of *Salvinia molesta* [24,25], which are covered by numerous trichome-like microstructures. Inspired by plants or animals from nature, many artificial structures have been invented and embedded in technical surfaces [8,9] to achieve oil/water separation. Previous publications have already reported outstanding oil/water separation performance on artificial surfaces with microstructures, including nanofur [26,27], nanofibers [28,29], or microparticles/powders [30,31]. However, the influence of structural dimensions such as size, spacing, or height/diameter ratio on selective wetting properties was rarely studied. In addition, most research focused on improving surface superhydrophobicity by topographical structures but ignored the function of cross-sectional architectures for enhancing oil absorption. Porous microstructures similar to sponges at the cross-section will very likely benefit oil absorbing volume and oil retention ability. Combining both surface structures and cross-sectional architecture might offer a new solution for highly efficient oil/water separation. Also, the dimension of these microstructures needs to be optimized to improve the oil/water separation ability.

In this paper, we developed a novel polyurethane (PU) foil by imprinting micropillar arrays on the surface and fabricating microporous structures at the cross-section for efficient oil/water separation. The resulting foil demonstrates excellent superhydrophobicity and superoleophilicity, leading to fascinating oil/water separation and oil retention capability. The effects of pillar spacing, height/diameter ratio, as well as pore size on the water and oil contact angles were analyzed. The oil absorption capacity of samples with different pore sizes or porosity was evaluated. The developed structured foil shows superior oil absorption efficiency and oil retention ability compared to a flat reference. Our study presents a facile method of manufacturing high-performance oil absorption foil for spilled oil collection.

2. Experimental Methods

2.1. Materials and Microstructure Fabrication

PU was used for microstructure fabrication because it is a common material for foaming [1,8,9] or nanoimprinting [32], possessing suitable mechanical and thermal properties for our experimental setup. Micropillar and microporous structured PU foils were produced from commercial thermoplastic PU sheets (DPS650, Jiejiayou materials Co., Ltd., Shenzhen, China) with a thickness of 1 mm. The glass transition temperature (T_g) of the polymer was 75 °C, which was obtained from producer. The purchased PU sheets were cut into small chips (30 mm × 20 mm) and clamped by two pieces of silicon template (30 mm × 20 mm), which was manufactured with post hole arrays (negative to micropillars) on the whole surface (Feimi Laser Technology Co., Ltd., Shanghai, China). The nearest neighbor spacing of the post hole array was customized as 5 µm, 10 µm, or 15 µm. The diameter of the holes was about 5 µm. The stepwise depth ranged from 1 µm to 12.5 µm to achieve a height/diameter aspect ratio (*AR*) of 0.2–2.5. Micropillar structures were embedded onto the PU chip by imprinting (hot embossing process [32]) on a home-built setup, which was similar to our prior work [32,33]. This method resulted in a PU foil with fully covered micropillars (the squeezed-out material from the edges without pillars was cut off, resulting in a size of about 30 mm × 20 mm × 0.3 mm). Silicon templates were used for such imprinting under a pressure of 5 MPa and a temperature of 80 °C for about

1 min. After that, the whole setup was put into a home-built high-pressure cell, which was connected to a carbon dioxide (CO_2)-supplying device. Compressed CO_2 was pumped into the cell, achieving a saturation pressure of up to 20 MPa. The temperature of the inner autoclave was controlled at 60 °C by a heating system to realize the supercritical state of CO_2 (above a pressure of 7.38 MPa and a temperature of 31.1 °C [34]), wherein CO_2 exhibits a liquid-like density and a gas-like diffusivity, allowing for rapid absorption by the polymer. After about 15 min of saturation, a rapid pressure quench (1 s) was triggered, yielding the foaming (lasts within 30 s) of PU foil with numerous micro-sized pores at cross-section. The foil thickness increased to around 1 mm after foaming. After cooling down the whole setup, the micropillar array was obtained on the PU surface by demolding the silicon templates. The fabricated foil was subsequently cleaned by high-pressure air and stored in the ambient environment.

2.2. Characterization Methods

The topography of the silicon template was imaged by an optical microscope (NX30-HK830, AOSV, Shenzhen, China). The micropillar arrays and cross-sectional porous microstructures were characterized by a scanning electron microscope (SEM, Ultra 60VP, Zeiss, Germany). The cross-section of the foil was obtained through the brittle fracture of foil by liquid nitrogen, as described in [35]. Pore size distribution were analyzed by the software ImageJ in SEM images. Three samples fabricated at different foaming conditions were imaged, and on each sample, five arbitrary positions in the central region of the cross-section were investigated. The pore dimensions in each image were accordingly measured and statistically analyzed, resulting in an average pore size for each experiment. From these averages, a mean value was determined to characterize the pore size obtained at a specific foaming condition. The porosity was calculated as the ratio of the pore volume to the volume of the foamed sample from micro-computed tomography (Xm-Tracer-uCT-90, IHEP, Beingjing, China). The diameter and depth of the post holes in the silicon template were determined by a laser microscope (Olympus LEXT OLS5100, Olympus Co., Ltd., Tokyo, Japan). The water or oil contact angle on the foil was measured by a SINDIN contact angle instrument (SDC2111071, Shengding Precision Instrument Co., Ltd., Dongguan, China). The droplet volume used in the contact angle measurements was 1 μL.

2.3. Oil/Water Separation Experiment

Motor oil (Shell Gadinia 40, Meideke Lubrication Oil Co., Ltd., Wuhan, China) was used in the oil/water separation experiment, wherein the water was dyed with methylene blue and the oil was dyed with Oil Red O (Yabang dying Co., Ltd., Changzhou, China). The fabricated PU foil was clamped by a tweezer and immersed in an oil spill on the water surface to absorb oil. The mass of the PU foil was measured by an electronic balance (XPR404S/AC, Mettler Toledo, Shanghai, China) before and after the oil/water separation experiment to calculate the oil absorption capacity, as follows:

$$\eta = (m_{after} - m_{before})/m_{before} \times 100\%. \quad (1)$$

The absorption time was counted once the foil contacted the oil, until full absorption (the foil color becomes dark red). The absorption efficiency was defined as the absorption capacity divided by the absorption time.

3. Results and Discussion

3.1. Fabrication of Micropillar and Microporous Structures onto PU Foil

The fabrication procedure of the topographical micropillar structures as well as microporous structures at the cross-section of PU foil is schematically illustrated in Figure 1. Silicon templates, covered by arrays of post hole microstructures (negative to the micropillar arrays, see Figure 1g), were used to imprint micropillars (Figure 1a). Applying a temperature of 80 °C and a pressure of 5 MPa, PU melted and flowed into the post holes, yielding micropillar arrays on the surface (Figure 1b). Pressure-induced saturation [36]

with supercritical CO_2 was employed to generate microporous structures inside the PU. This method produced pores at the cross-section but left a thin free layer close to surface, which might have been caused by constraint from the post holes in the silicon template. Such constraint probably inhibited the pore growth near the pillar surface. The thickness of such a pore-free layer was about 25 µm, as shown in Figure 1f. Increasing the saturation pressure up to 20 MPa and temperature to 60 °C led to the dissolution of CO_2 within PU. After a rapid pressure quenching, CO_2 nucleated into many tiny pores (Figure 1c) and the pore size gradually grew (i.e., forming process) by CO_2 diffusion (Figure 1d). Finally, micropillar and microporous structures were obtained on the PU foil after cooling down the whole setup and demolding (Figure 1e). Pillar dimension such as side-to-side spacing (*s*), height (*h*), as well as diameter (*d*) are defined in Figure 1h. Figure 1i shows an optical photograph of the fabricated microstructured PU foil. The foil appeared translucent due to the light regulation by micropillars and pores. The foil size was around 30 mm × 20 mm × 1 mm.

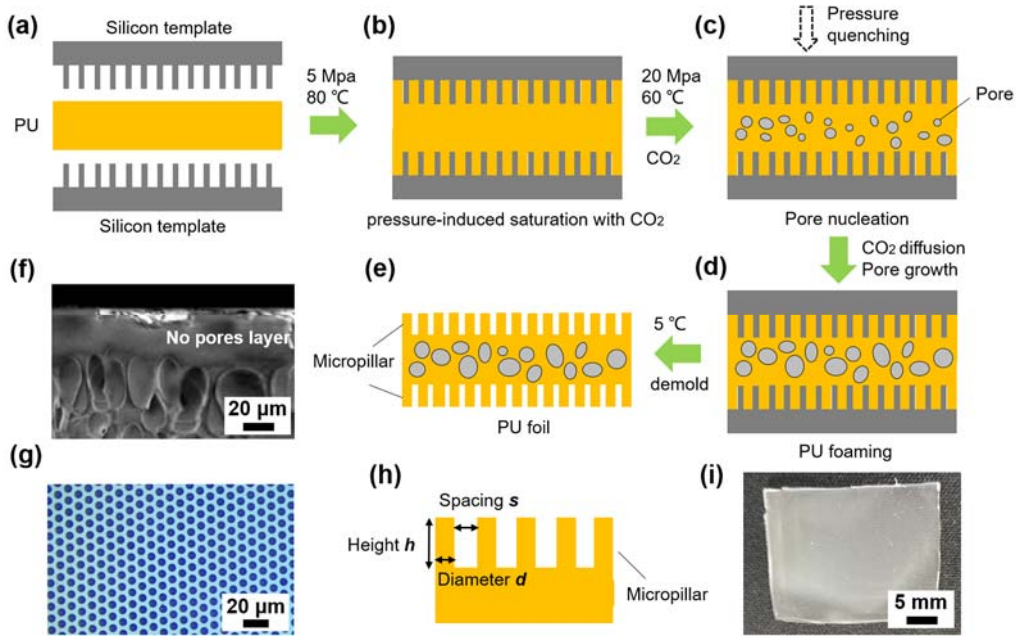

Figure 1. Schematic procedure of the developed approach for fabricating micropillar and microporous structures on PU foil. (**a**) Flat PU chip between two silicon templates. (**b**) The whole setup was put into a supercritical CO_2 environment for saturation. (**c**) Pressure quenching and depressurization caused CO_2 to nucleate into numerous tiny pores within the polymer. (**d**) Pore size grew (foaming) with CO_2 diffusion. (**e**) The resulting PU foil showed a micropillar array on the surface and micropores at the cross-section. (**f**) SEM image indicating the free layer (about 25 µm thickness) without pores below the pillars. (**g**) Post hole array in hexagonal lattice on the topography of the silicon template. (**h**) Specifications of micropillar array. (**i**) A photo of the fabricated PU foil. For clarity, the schematic foil in (**a**–**e**) is not to scale and the thickness decrease after nanoimprinting as well as the volume increase due to foaming is not shown.

3.2. Structural Properties

SEM micrographs of the pillar topography and the porous cross-section of the fabricated PU samples are shown in Figure 2, taking the example of three different pillar spacings (*s* = 5 µm (a, compacted), 10 µm (b), and 15 µm (c, spacious)). The pillar diameter was kept constant as 5 µm. The height of the pillars obtained was approximately 12.5 µm, 3.75 µm, and 5 µm, thus the respective aspect ratios shown here amounted to (a) 2.5, (b) 0.75, and (c) 1, respectively. Although the pillar height was sometimes slightly larger than the hole depth on the silicon template due to the tension forces during demolding, in most cases, the pillar height approximated the hole depth. Samples with dedicated spacing and

aspect ratio were fabricated and characterized before the oil/water separation experiments. Nonetheless, it is also worth mentioning that the pillars with too high aspect ratio would bend or buckle during demolding (e.g., Figure 2a), potentially leading to worse selective wetting performance. Figure 2d–f show the pore structure of the PU sample prepared under different foaming pressures of 20 MPa, 18 MPa, and 16 MPa, resulting in average pore sizes of about 50 μm, 75 μm, and 125 μm, respectively. The SEM micrographs were taken in the central region of the cross-section. Reduced foaming pressure generally yielded increasing pore size within a reasonable pressure range, while the pore size could not be unlimitedly increased. This trend followed the homogeneous nucleation theory in [37], which indicated reduced pore size but higher pore density with increased foaming pressure. In our study, the obtained pore size was mainly in the range of 20 μm to 150 μm.

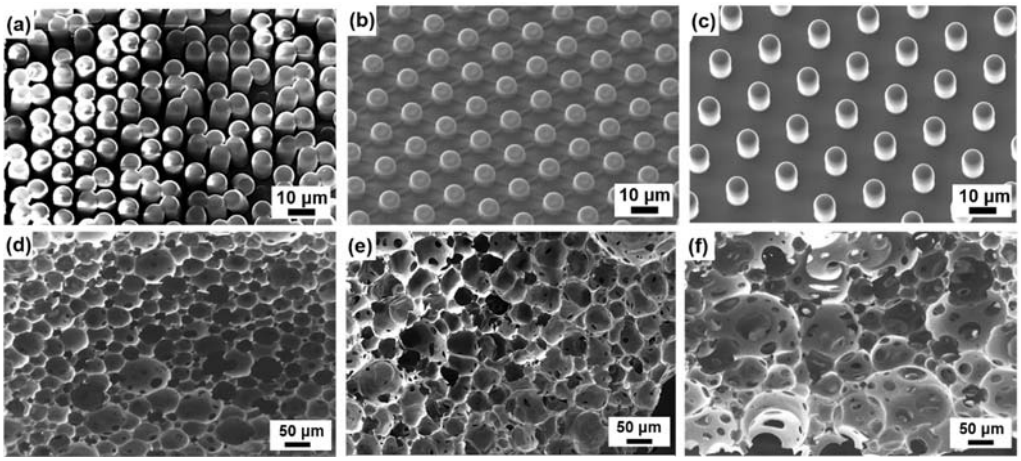

Figure 2. SEM images of the topographical micropillar arrays as well as the cross-sectional microporous structures on the PU foil. Pillar spacings of (**a**) 5 μm, (**b**) 10 μm, and (**c**) 15 μm were fabricated. The respective height of pillars was tailored, resulting in aspect ratios of 2.5, 0.75, and 1. The imprinting condition for the three surfaces was the same (80 °C and 5 MPa for 1 min). With the cross-sectional samples, the average pore sizes (taken in the center of foil cross-section) amounted to (**d**) 50 μm, (**e**) 75 μm, and (**f**) 125 μm, obtained at the foaming pressures of 20 MPa, 18 MPa, and 16 MPa, respectively. The saturation temperature was the same for three samples (60 °C). The overall thicknesses of three foamed PU foils were also similar (approximately 1 mm).

Figure 3 summarizes the pore size distribution at the cross-section of three different foils (corresponding to Figure 2d–f, respectively), which were fabricated under stepwise reduced foaming pressure. One can observe that the pore size on each foil manifested a similar Gaussian distribution pattern. It seems that the CO_2 foaming process generated regularly distributed micropores independent of the foaming conditions. However, the Gaussian peak for each sample was located at a distinct position. Interestingly, the width of the Gaussian distribution also varied in terms of individual foil. The average pore size and its corresponding deviation were calculated and are shown in the figure legend. The sample with a larger pore size generally showed a wider distributing pattern. As a result, the calculated average pore size for each sample differed. Such a difference was triggered by the different foaming pressure of each sample, i.e., high pressure reduced the pore size and improved their uniformity.

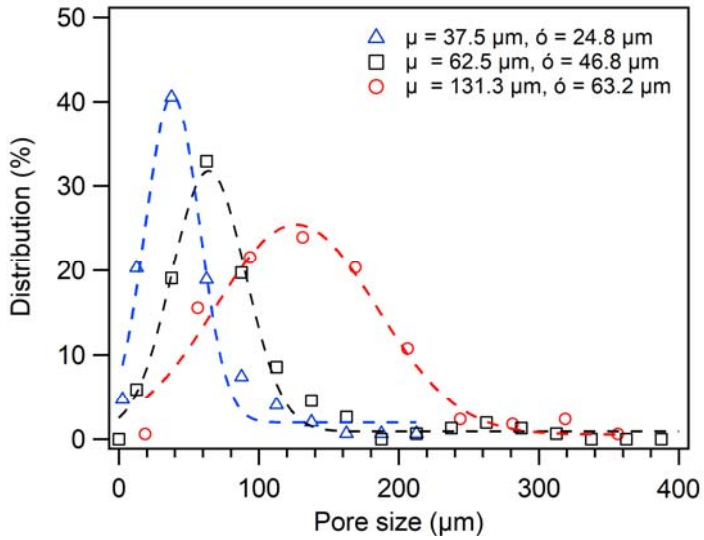

Figure 3. Pore size distribution at the cross-section for three different PU foils. A similar Gaussian distribution pattern was observed for all samples, whereas the average pore size differed. The average value μ and its corresponding standard deviation σ of each dataset are shown in the legend. The dashed curve is the corresponding fitting trend to each dataset. The foaming pressures for samples showing pore sizes from small to large were 20 MPa, 18 MPa, and 16 MPa, respectively. The foaming temperature was 60 °C.

3.3. Selective Wetting Property

Water and oil contact angles on the fabricated PU foil were characterized to examine its hydrophobic and oleophilic properties. Considering that micropillars might fracture or even totally detach from the foil surface (although in a small area) in upscaled applications, a superhydrophobic and superoleophilic foil cross-section is also important for oil/water separation. Thus, the results of the micropillar surface and microporous cross-section are summarized and compared to a pristine reference (i.e., flat bulk sample). Figure 4a,b show the water and oil droplets on the flat PU surface. Corresponding results of the micropillar surface and microporous cross-section of a structured foil are revealed in Figure 4c–f, respectively. Apparently, all of the samples showed a selective wetting property, i.e., a comparably large water contact angle while a relatively small oil contact angle. Nevertheless, it is interesting to note that for micropillar and microporous structures, the disparity between the water and oil contact angles further widened if compared to the flat foil. More specifically, the water contact angle significantly increased from 110° to around 150°, whereas the oil contact angle evidently declined from 52° to about 20° after embedding microstructures. The surface roughness of flat foil might also cause potential variations in contact angle, which was observed to be very small in our experiments (please see the error bars in Figure 5). However, this effect did not influence the overall trend of our results, i.e., microstructures triggered selective wetting. Thus, we conclude that topographical micropillar arrays and cross-sectional micropores could immensely enhance the hydrophobicity and oleophilicity (selective wetting property) of PU foil. The corresponding contact angle values also indicated the fascinating superhydrophobicity and superoleophilicity of our developed PU foil, which implied superior oil/water separating performance.

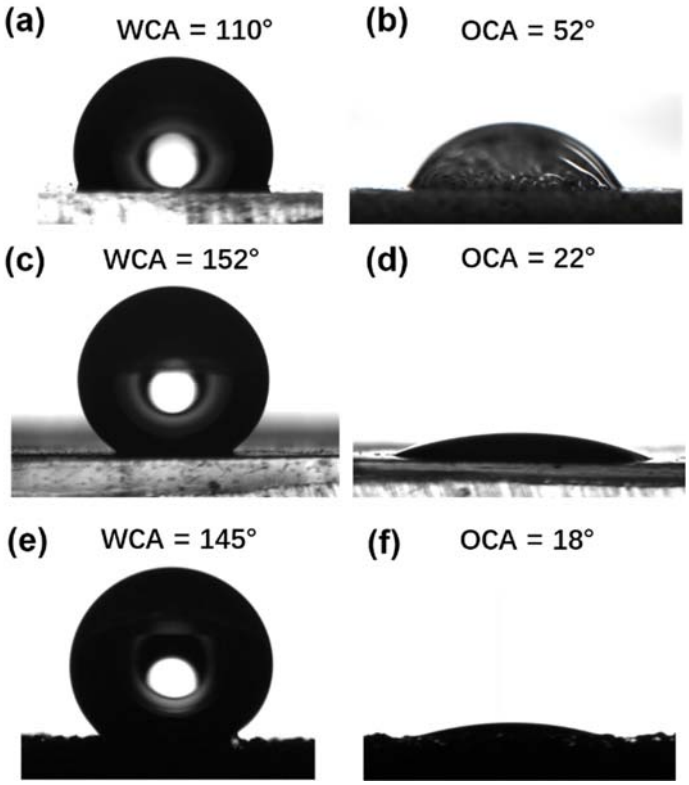

Figure 4. Picture of water (left column) and oil (right column) droplets on the PU foil. (**a**) Water and (**b**) oil contact angles on a flat PU surface. (**c**) Water and (**d**) oil contact angles on a micropillar surface. The pillar spacing is 5 μm. The respective height of the pillars is 5 μm, resulting in an aspect ratio of 1. (**e**) Water and (**f**) oil contact angles on microporous cross-section of a PU foil. The average pore size of the specific sample used in the experiment is around 126 μm. The droplet volume is 1 μL.

The dimensions of microstructures might affect the superhydrophobicity and superoleophilicity of the developed foil. Hence, the water and oil contact angles were further analyzed on samples with different pillar spacings, height/diameter ratios, or pore sizes. First, foils with pillar spacings of 5 μm, 10 μm, and 15 μm were tested and the results were compared to a flat surface (see Figure 5a). Consistent with Figure 4, all of the micropillar surfaces displayed higher water contact angles but lower oil contact angles than the flat reference. Among them, the sample with 5 μm pillar spacing demonstrated the most excellent superhydrophobicity and superoleophilicity. In terms of samples with 10 μm and 15 μm spacing, the selective wetting effect was slightly weakened compared to the foil with 5 μm spacing, i.e., the difference between water and oil contact angles was reduced. Moreover, the results for these two samples (10 μm and 15 μm spacing) were similar. Pillar spacing smaller than 5 μm might have led to a more apparent selective wetting effect. Nonetheless, such a dimension usually requires high-precision imprinting mold and also has the risk of pillar fracture or buckling during demolding. Thus, to achieve a robust selective wetting ability for oil/water separation, the subsequent PU foils were all fabricated with micropillars with 5 μm spacing.

The *AR* of the micropillars was also tailored to analyze its influence on the selective wetting performance. The results are summarized in Figure 5b. The water contact angle increased with rising *AR* until reaching a plateau at around 150°. On the contrary, the oil contact angle manifested a reducing trend before stabilizing at around 20°. For the aim of achieving both superhydrophobicity and superoleophilicity on the foil, the *AR* of the micropillars was expected to be higher than 0.75. Similar to pillar spacing, too high *AR* generally requires an elaborated fabrication procedure and is prone to fracturing and buckling during demolding, which might also attenuate the selective wetting performance. Thus, an eligible *AR* of 1 was adopted in the following study. This outcome indicated

structural parameters of s = 5 μm and AR = 1 for the micropillar arrays to achieve strong selective wetting for oil/water separation.

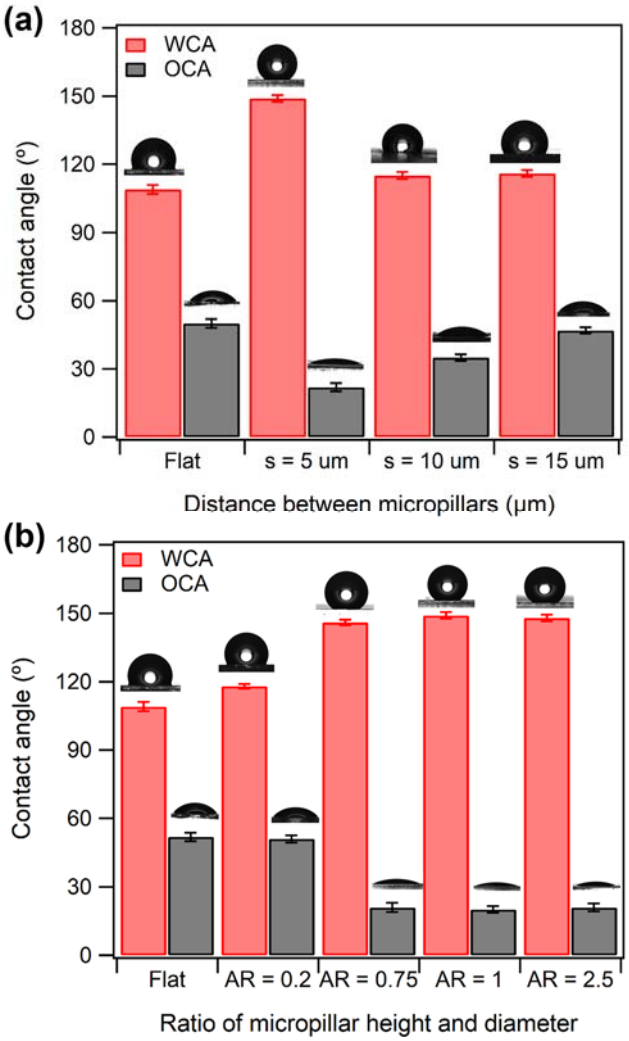

Figure 5. Influence of (**a**) micropillar spacing and (**b**) height/diameter ratio on the selective wetting property of PU foil. In (**a**) the pillar height is kept constant at 5 μm (i.e., AR = 1). In (**b**) the pillar spacing remains 5 μm on different samples. For each sample, three measurements were conducted at arbitrary positions. The average values and corresponding statistical error are shown as columns and error bars in the figure.

As already illustrated in Figure 4, cross-sectional porous structures also enhanced the water repellency of PU. However, the pore distribution differed among samples foaming under different saturation pressures. Such a characteristic might also cause variations in the wetting property. Hence, the water contact angles on the porous cross-section of foils demonstrating varied pore sizes were characterized and are shown in Figure 6. The results of the oil contact angles were not plotted because all of the porous samples revealed a similar value of around 20°. One can observe that the water contact angles fluctuated among porous samples but were all larger than that on the bulk reference. It seems that the pore size did not exhibit a regular dependency on water repellency or oil attraction. The function of pore size might be to tune the oil absorption volume or rate, which will be discussed in the next section.

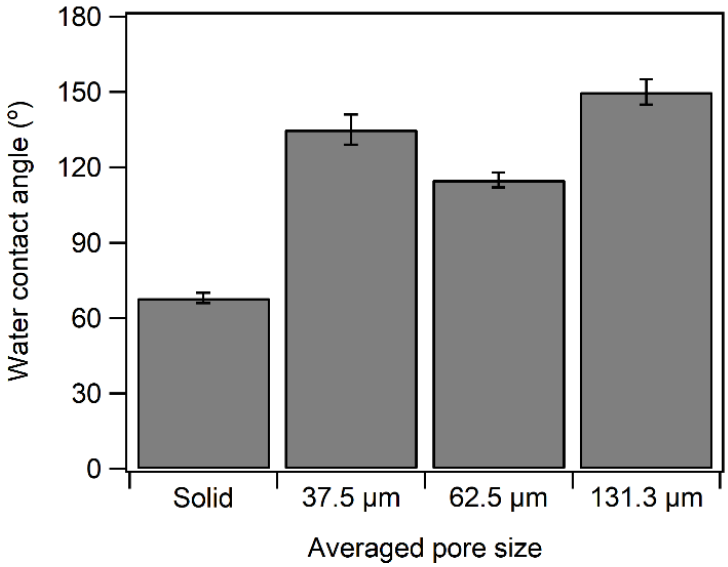

Figure 6. Water contact angle on the porous cross-section of PU foil with different pore sizes. The result of a bulk sample was plotted as a comparison. Each bar in the figure represents an average value from three arbitrary measurements. The error bar is the corresponding statistical error.

3.4. Oil/water Separation

The fabricated structured PU foil was applied to remove the oil spill from water. Figure 7 shows the time-lapse of oil absorption by the foil. Once the foil contacted the oil, the oil spill (dyed in red) was quickly and completely absorbed within 10 s from water (dyed in blue), which was thereafter dabbed away from the water surface. This timescale was comparable to the results in references [11,24]. Although the experimental conditions (e.g., oil type or amount) employed by us and in the references were not exactly the same, this outcome proved the excellent oil/water separation ability of our developed PU foil. To further investigate its maximum absorption capacity, the foil was subsequently immersed into a large amount of oil spill to achieve full absorption. After nearly 20 s, a maximum absorption volume was reached (nearly 400% weight of the original foil), indicating a high absorption efficiency.

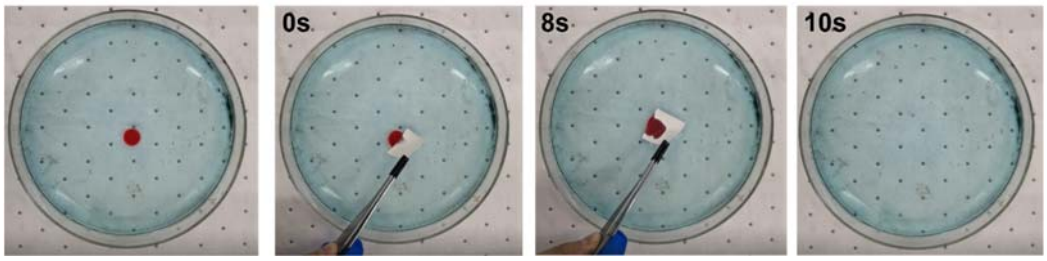

Figure 7. Time-lapse of the developed PU foil absorbing oil (in red) in water (in blue). The oil spill was completely removed within 10 s. A micropillar array of s = 5 μm and AR = 1 was fabricated on the foil surface. The average pore size at the foil cross-section of the specific sample used in this experiment was around 124.6 μm.

More specifically, the absorption capacity of the structured PU foil was quantitatively evaluated and plotted as a function of the average pore size at the cross-section (Figure 8a). The corresponding result of a flat, bulk foil is compared. With no pores at the cross-section, the oil absorption capacity of pristine PU foil was only less than 20%. Upon the introduction of porous microstructures, however, the oil absorption capacity significantly rose to several hundred percent, depending on the pore size. Larger pores usually allow higher oil absorption capacity. This outcome confirmed that cross-sectional porous microstructures

mainly functioned as numerous tiny oil containers to enhance the oil absorption capacity. According to nucleation theory proposed by [37], lower foaming pressures allow increasing pore size but reduce the pore density, which also affects oil absorption capacity. Thus, porosity was calculated as the ratio of total pore volume to the foamed PU volume, which was dominated by both pore size and pore density. The impact of porosity on the oil absorption ability was analyzed (see Figure 8b). A similar increasing trend with pore size was observed. This was reasonable because high porosity is supposed to offer more containers for oil storage, which will lead to more oil absorption volume. In terms of our fabrication method, the pore size and porosity could be tailored by adjusting the saturation pressure or temperature during the supercritical CO_2 foaming process. Nevertheless, both parameters could not be unlimitedly increased due to the actual implemental restraints of experimental conditions and the thickness of untreated foil. The largest absorption capacity of around 500% was accomplished by a structured foil with an average pore size of about 130 μm and porosity of nearly 90%. Such performance was superior to the results of typical mesh sorbents [22,23], but not as profitable as polymeric sponges [7,18]. It is worth mentioning that such a comparison is extremely rough because the absorption capacity calculated from the mass was significantly influenced by the original weight of the sorbent (e.g., lighter sorbents are more likely to obtain higher absorption capacity). Nonetheless, our results demonstrate the excellent oil-absorbing capability of the developed PU foil.

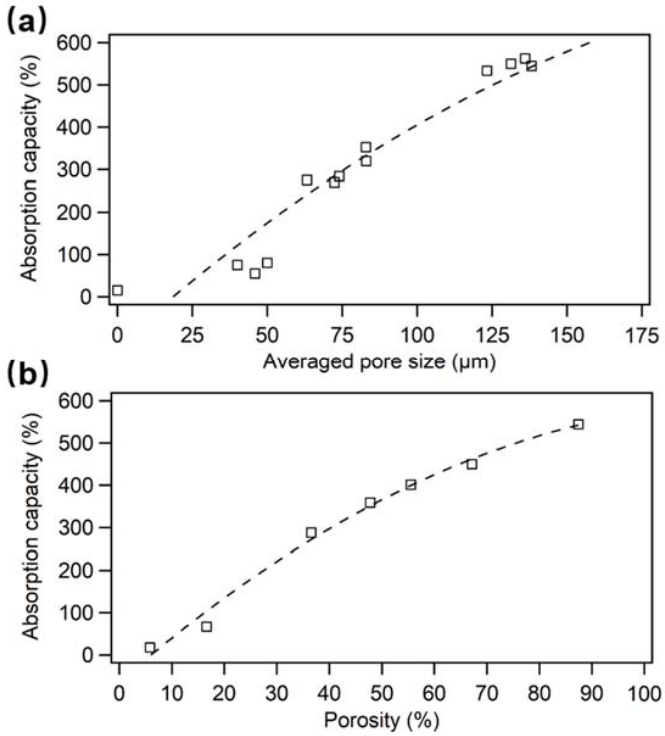

Figure 8. Oil absorption capacity plotted as a function of (**a**) pore size and (**b**) porosity at the cross-section of the structured PU foil. On all examined samples, a micropillar array of s = 5 μm and AR = 1 was fabricated on the surface. Each data point in the figure represents the measured absorption capacity of a newly fabricated, single-use foil. The foaming pressure for these foils ranged from 16 MPa to 20 MPa.

Finally, the oil absorbing performance (i.e., rate and capacity) of the structured PU foil was compared to a flat, bulk reference. As displayed in Figure 9a, both foils reached their full absorption within some seconds, while the absorbed maximum oil volume significantly differed. Although taking a longer absorption time, our structured foil demonstrated a dramatically higher absorption capacity than the unstructured foil of the same material. To carry out a quantitative comparison by a single parameter, the absorption efficiency

of both foils was calculated. The results revealed 15.7% per second for the structured foil but only 4.4% per second for the unstructured sample. This indicated a nearly 4 times improvement of oil absorption efficiency owing to the introduction of micropillar and microporous structures to the PU foil. Moreover, the oil retention time within both foils was also evaluated and compared (Figure 9b). As both foils reached maximum absorption within 30 s (see Figure 9a), the starting time for this long-term retention evaluation was set to 30 s. After that, the absorbed oil was constantly retained within the structured PU foil in the subsequent 7 days, demonstrating a stabilized absorption capacity of above 400%. However, the oil absorption capacity of the unstructured foil gradually reduced from 42% to 12% over the same time period. This was probably due to oil loss from the surface of the flat foil, where oil residuals were temporarily adhered but not completely absorbed in the inner foil during absorption. Oil detached from the foil due to gravity over time, leading to lower oil retention by the foil. Consequently, it can be concluded that our developed micropillar and microporous PU foil showed superior oil absorption efficiency and oil retention ability if compared to the unstructured sample, making it an ideal element for oil/water separation applications. Moreover, our method was facile and environmentally friendly, showing great compatibility for other thermoplastic polymers. Nonetheless, dedicated experimental conditions (e.g., temperature or pressure) should be further studied. In terms of practical applications for industrial use, foil upscaling might be achieved by a roll-to-roll fabricating process [27], which allows the fabrication of large-sized polymeric foils with microstructures on the surface.

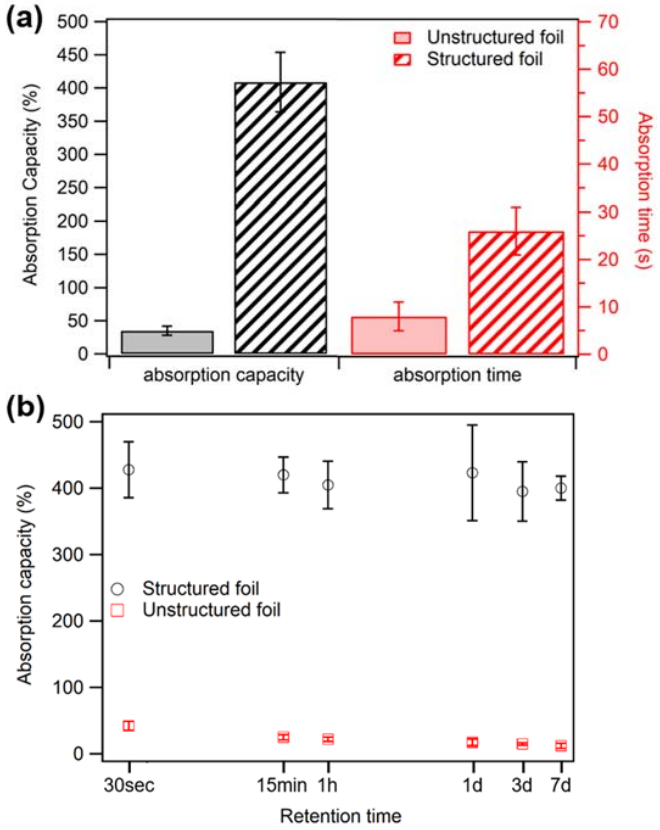

Figure 9. Comparison of oil absorbing performance between the structured and unstructured PU foils. (**a**) Absorption capacity and time. (**b**) Absorption capacity as a function of oil retention time within both foils. The time axis is plotted as a logarithmic scale in (**b**) for easy illustration. The structured foil possessed a micropillar array of s = 5 μm and AR = 1 on the surface. The mean pore size at the cross-section was characterized as around 130 μm. Both foils were stored under ambient conditions (25 °C, in air) during the long-term retention experiment. Each experiment was conducted with a new, single-use foil.

4. Conclusions

To conclude, we developed a favorable PU foil simultaneously possessing micropillar arrays on the surface and microporous structures at the cross-section for efficient oil/water separation. Such a structured foil demonstrated excellent superhydrophobicity and superoleophilicity, resulting in a remarkable improvement in oil absorption efficiency by nearly 4 times if compared to the unstructured pristine foil. The structured foil also showed superior oil retention ability as long as 7 days, during which the oil absorption capacity stabilized as high as nearly 400%. Moreover, the fabrication and usage of such foil was achieved by a purely mechanical and physical method, which was facile and environmentally friendly without any chemical pollution.

The micropillar arrays on the foil surface functioned as an isolated barrier to enhance water repellency and oil attraction (selective wetting). Specifically, the effects of pillar spacing and the height/diameter ratio on water and oil contact angles were investigated. Pillar spacing at 5 μm and an aspect ratio of 1 were summarized for the aim of achieving robust selective wetting performance. Porous microstructures at the foil cross-section also benefitted the increase in water contact angle, whereas the pore size and porosity mainly contributed to oil absorption, like storage containers, with an almost linear relationship. Nevertheless, the pore size and porosity were limited within a maximum value depending on the CO_2 foaming pressure and temperature. This study presents a rapid and reproducible approach for fabricating oil/water separation foils, and more importantly, our approach is also compatible with other oil absorption polymers.

Author Contributions: Conceptualization, W.W. and X.Y.; methodology, M.X.; investigation, Q.W.; writing—original draft preparation, W.W.; writing—review and editing, W.W. and Q.W.; supervision, C.S.; funding acquisition, W.W., M.X. and C.S. All authors have read and agreed to the published version of the manuscript.

Funding: This research was funded by the Natural Science Foundation of Hubei Province (2022CFB866), the Natural Science Foundation of China (52105496, 52171328), the National Defense Project for Foundation Enhancement, and the Foundation of National Key Laboratory on Ship Vibration and Noise (JCKY2021207CI03).

Institutional Review Board Statement: Not applicable.

Informed Consent Statement: Not applicable.

Data Availability Statement: Data are contained within the article.

Acknowledgments: This work was financially supported through the Natural Science Foundation of Hubei Province (2022CFB866), the Natural Science Foundation of China (52105496, 52171328), and the National Defense Project for Foundation Enhancement. W.W. gratefully acknowledges support from the Foundation of National Key Laboratory on Ship Vibration and Noise (JCKY2021207CI03).

Conflicts of Interest: The authors declare no conflicts of interest.

References

1. Zhang, N.; Qi, Y.; Zhang, Y.; Luo, J.; Cui, P.; Jiang, W. A Review on Oil/Water Mixture Separation Material. *Ind. Eng. Chem. Res.* **2020**, *59*, 14546–14568. [CrossRef]
2. Laurel, B.J.; Copeman, L.A.; Iseri, P.; Spencer, M.L.; Hutchinson, G.; Nordtug, T.; Donald, C.E.; Meier, S.; Allan, S.E.; Boyd, D.T.; et al. Embryonic Crude Oil Exposure Impairs Growth and Lipid Allocation in a Keystone Arctic Forage Fish. *iScience* **2019**, *19*, 1101–1113. [CrossRef] [PubMed]
3. Nordvik, A.B.; Simmons, J.L.; Bitting, K.R.; Lewisa, A.; Kristiansen, T.S. Oil and water separation in marine oil spill clean-up operations. *Spill Sci. Technol. Bull.* **1996**, *3*, 107–122. [CrossRef]
4. Tansel, B.; Regula, J. Coagulation enhanced centrifugation for treatment of petroleum hydrocarbon contaminated waters. *J. Environ. Sci. Health Part A Toxic Hazard. Subst. Environ. Eng.* **2000**, *35*, 1557–1575. [CrossRef]
5. Kota, A.K.; Kwon, G.; Choi, W.; Mabry, J.M.; Tuteja, A. Hygro-responsive membranes for effective oil–water separation. *Nat. Commun.* **2012**, *3*, 1025. [CrossRef] [PubMed]
6. Ahmed, F.E.; Lalia, B.S.; Hilal, N.; Hashaikeh, R. Underwater superoleophobic cellulose-electrospun PVDF–HFP membranes for oil/water separation. *Desalination* **2014**, *344*, 48–54. [CrossRef]

7. Yu, C.; Yu, C.; Cui, L.; Song, Z.; Zhao, X.; Ma, Y.; Jiang, L. Facile Preparation of the Porous PDMS Oil-Absorbent for Oil/Water Seperation. *Adv. Mater. Interfaces* **2017**, *4*, 1600862. [CrossRef]
8. Gupta, R.K.; Dunderdale, G.J.; England, M.W.; Hozumi, A. Oil/water separation techniques: A review of recent progresses and future directions. *J. Mater. Chem. A* **2017**, *5*, 16025. [CrossRef]
9. Wang, B.; Liang, W.; Guo, Z.; Liu, W. Biomimetic superlyophobic and superlyophilic materials applied for oil/water separation: A new strategy beyond nature. *Chem. Soc. Rev.* **2015**, *44*, 336–361. [CrossRef] [PubMed]
10. Wang, D.; Liu, S.; Dong, B.; Yuan, L.; Pan, H.; Zhao, Q. Research Progress on Factors Affecting Oil-Absorption Performance of Cement-Based Materials. *Materials* **2023**, *16*, 3166. [CrossRef] [PubMed]
11. Farshad, B.; Hossein, K.; Masoud, S. Recyclable magnetic superhydrophobic straw soot sponge for highly efficient oil/water separation. *J. Colloid Interface Sci.* **2017**, *497*, 57–65.
12. Kovummal, G.; Pattayil, A. Coconut shell based activated carbon–iron oxide magnetic nanocomposite for fast and efficient removal of oil spills. *J. Environ. Chem. Eng.* **2015**, *3*, 2068–2075.
13. Zhang, T.; Li, Z.; Lü, Y.; Liu, Y.; Yang, D.; Li, Q.; Qiu, F. Recent progress and future prospects of oil-absorbing materials. *Chin. J. Chem. Eng.* **2019**, *27*, 1282–1295. [CrossRef]
14. Saman, S.; Shabnam, S.; Hossein, A.; Pooya, J.; Majid, A. Fabrication of novel chitosan/PAN/magnetic ZSM-5 zeolite coated sponges for absorption of oil from water surfaces. *Int. J. Biol. Macromol.* **2017**, *105*, 370–376.
15. Liu, Z.; Qin, Z.; Zhao, G.; Aladejana, J.; Wang, H.; Huang, A.; Chen, D.; Xie, Y.; Peng, X.; Chen, T. High-efficiency oil/water absorbent using hydrophobic silane-modified plant fiber sponges. *Compos. Commun.* **2021**, *25*, 100763. [CrossRef]
16. Chen, T.; Li, M.; Zhou, L.; Ding, X.; Lin, D.; Duan, T.; Yang, G.; He, R.; Zhu, W. Bio-Inspired Biomass-Derived Carbon Aerogels with Superior Mechanical Property for Oil−Water Separation. *ACS Sustain. Chem. Eng.* **2020**, *8*, 6458–6465. [CrossRef]
17. Ma, L.; Lv, H.; Yu, H.; Kong, L.; Zhang, R.; Guo, X.; Jin, H.; He, G.; Liu, X. In-depth investigation on the factors affecting the performance of high oil-absorption resin by response surface method. *Chin. J. Chem. Eng.* **2021**, *33*, 286–296. [CrossRef]
18. Li, J.; Xu, C.; Zhang, Y.; Wang, R.; Zha, F.; She, H. Robust superhydrophobic attapulgite coated polyurethane sponge for efficient immiscible oil/water mixture and emulsion separation. *J. Mater. Chem. A* **2016**, *4*, 15546–15553. [CrossRef]
19. Wang, X.; Pan, Y.; Liu, X.; Liu, H.; Li, N.; Liu, C.; Schubert, D.W.; Shen, C. Facile Fabrication of Superhydrophobic and Eco-Friendly Poly(lactic acid) Foam for Oil-Water Separation via Skin-Peeling. *ACS Appl. Mater. Interfaces* **2019**, *11*, 14362–14367. [CrossRef] [PubMed]
20. Wang, X.; Pan, Y.; Shen, C.; Liu, C.; Liu, X. Facile Thermally Impacted Water-Induced Phase Separation Approach for the Fabrication of Skin-free Thermoplastic Polyurethane Foam and Its Recyclable Counterpart for Oil-water Separation. *Macromol. Rapid Commun.* **2018**, *39*, 1800635. [CrossRef] [PubMed]
21. Gao, C.; Sun, Z.; Li, K.; Chen, Y.; Cao, Y.; Zhang, S.; Feng, L. Integrated Oil Separation and Water Purification by a Double-Layer TiO2-Based Mesh. *Energy Environ. Sci.* **2013**, *6*, 1147–1151. [CrossRef]
22. Wang, G.; Zeng, Z.; Wang, H.; Zhang, L.; Sun, X.; He, Y.; Li, L.; Wu, X.; Ren, T.; Xue, Q. Low Drag Porous Ship with Superhydrophobic and Superoleophilic Surface for Oil Spills Cleanup. *ACS Appl. Mater. Interfaces* **2015**, *7*, 26184–26194. [CrossRef] [PubMed]
23. Li, J.; Kang, R.; Zhang, Y.; Li, M.; She, H.; Zha, F.; Lei, Z. Facile fabrication of superhydrophobic meshes with different water adhesion and their influence on the oil/water separation. *RSC Adv.* **2016**, *6*, 90824–90830. [CrossRef]
24. Zeiger, C.; Silva, I.C.R.; Mail, M.; Kavalenka, M.N.; Barthlott, W.; Hölscher, H. Microstructures of superhydrophobic plant leaves—Inspiration for efficient oil spill cleanup materials. *Bioinspir. Biomim.* **2016**, *11*, 0560003. [CrossRef] [PubMed]
25. Yang, Y.; Li, X.; Zheng, X.; Chen, Z.; Zhou, Q.; Chen, Y. 3D-Printed Biomimetic Super-Hydrophobic Structure for Microdroplet Manipulation and Oil/Water Separation. *Adv. Mater.* **2018**, *30*, 1704912. [CrossRef] [PubMed]
26. Röhrig, M.; Mail, M.; Schneider, M.; Louvin, H.; Hopf, A.; Schimmel, T.; Worgull, M.; Hölscher, H. Nanofur for Biomimetic Applications. *Adv. Mater. Interfaces* **2014**, *1*, 1300083. [CrossRef]
27. Weiser, P.; Kietz, R.; Schneider, M.; Worgull, M.; Hölscher, H. Roll-to-roll fabrication of superhydrophobic pads covered with nanofur for the efficient clean-up of oil spills. *Beilstein J. Nanotechnol.* **2022**, *13*, 1228–1239. [CrossRef] [PubMed]
28. Wang, X.; Yu, J.; Sun, G.; Ding, B. Electrospun nanofibrous materials: A versatile medium for effective oil water separation. *Mater. Today* **2016**, *19*, 403–414. [CrossRef]
29. Si, Y.; Yu, J.; Tang, X.; Ge, J.; Ding, B. Ultralight nanofibre-assembled cellular aerogels with superelasticity and multifunctionality. *Nat. Commun.* **2014**, *5*, 5802. [CrossRef] [PubMed]
30. Akhavan, B.; Jarvis, K.; Majewski, P. Hydrophobic Plasma Polymer Coated Silica Particles for Petroleum Hydrocarbon Removal. *ACS Appl. Mater. Interfaces* **2013**, *5*, 8563–8571. [CrossRef]
31. Zhu, Q.; Pan, Q. Mussel-Inspired Direct Immobilization of Nanoparticles and Application for Water-Oil Separation. *ACS Nano* **2014**, *2*, 1402–1409. [CrossRef] [PubMed]
32. Wu, W.; Guttmann, M.; Schneider, M.; Thelen, R.; Worgull, M.; Gomard, G.; Hölscher, H. Snake-Inspired; Nano-Stepped Surface with Tunable Frictional Anisotropy Made from a Shape-Memory Polymer for Unidirectional Transport of Microparticles. *Adv. Funct. Mater.* **2021**, *31*, 2009611. [CrossRef]
33. Wu, W.; Yu, S.; Schreiber, P.; Dollmann, A.; Lutz, C.; Gomard, G.; Greiner, C.; Hölscher, H. Variation of the frictional anisotropy on ventral scales of snakes caused by nanoscale steps. *Bioinspir. Biomim.* **2020**, *15*, 056014. [CrossRef] [PubMed]
34. Cooper, A. Polymer synthesis and processing using supercritical carbon dioxide. *J. Mater. Chem.* **2000**, *10*, 207–234. [CrossRef]

35. Wu, W.; Lutz, C.; Mersch, S.; Thelen, R.; Greiner, C.; Gomard, G.; Hölscher, H. Characterization of the microscopic tribological properties of sandfish (*Scincus scincus*) scales by atomic force microscopy. *Beilstein J. Nanotechnol.* **2018**, *9*, 2618–2627. [CrossRef] [PubMed]
36. Syurik, J.; Schwaiger, R.; Sudera, P.; Weyand, S.; Johnsen, S.; Wiegand, G.; Hölscher, H. Bio-inspired micro-to-nanoporous polymers with tunable stiffness. *Beilstein J. Nanotechnol.* **2017**, *8*, 906–914. [CrossRef] [PubMed]
37. Colton, J.; Suh, N. The nucleation of microcellular thermoplastic foam with additives: Part I: Theoretical considerations. *Polym. Eng. Sci.* **1987**, *27*, 485–492. [CrossRef]